Journal of Magnetic Resonance 210 (2011) 151–157

Contents lists available at ScienceDirect

Journal of Magnetic Resonance

journal homepage: www.elsevier.com/locate/jmr

Communication

The matrix formalism for generalised gradients with time-varying orientation in diffusion NMR

Ivana Drobnjak *, Hui Zhang, Matt G. Hall, Daniel C. Alexander

Center for Medical Image Computing, Department of Computer Science, University College London (UCL), Gower Street, London WC1E 6BT, United Kingdom

ARTICLE INFO

Article history:
Received 6 January 2011
Revised 24 February 2011
Available online 4 March 2011

Keywords:
Diffusion NMR
Microstructure
Matrix formalism
Gradient orientation
Rotating gradients
STEAM
dPFG

ABSTRACT

The matrix formalism is a general framework for evaluating the diffusion NMR signal from restricted spins under generalised gradient waveforms. The original publications demonstrate the method for waveforms that vary only in magnitude and have fixed orientation. In this work, we extend the method to allow for variations in the direction of the gradient. This extension is necessary, for example to incorporate the effects of crusher gradients or imaging gradients in diffusion MRI, to characterise signal anisotropy in double pulsed field gradient (dPFG) experiments, or to optimise the gradient waveform for microstructure sensitivity. In particular, we show for primitive geometries (planes, cylinders and spheres), how to express the matrix operators at each time point of the gradient waveform as a linear combination of one or two fundamental matrices. Thus we obtain an efficient implementation with both the storage and CPU demands similar to the fixed-orientation case. Comparison with Monte Carlo simulations validates the implementation on three different sequences: dPFG, helical waveforms and the stimulated echo (STEAM) sequence.

1. Introduction

The matrix formalism, introduced by Callaghan [1], is a powerful approach for evaluating the diffusion NMR signal under generalised waveforms for spins restricted by any geometry. The method is based on the multiple propagator approach developed by Caprihan [2], and it involves approximating the gradient waveform with an interleaved sequence of gradient impulses that change the phase of each spin and "empty" time intervals during which the spins diffuse. These events can be represented with matrices, namely A and S (phase evolution) and R (diffusive evolution), which need to be calculated only once for a particular geometry and a particular gradient waveform. The final signal then has closed form comprising a series product of powers of these matrices:

$$SRA^{m_2}RA^{m_3}\ldots RA^{m_N}RS^{*}, \tag{1}$$

where $m_i, i = 2, 3 \ldots N$ are integers and $*$ represents the hermitian operator.

So far, the matrix formalism has been mainly applied using Eq. (1) directly [3–5], which requires that the gradient impulse, and hence the gradient orientation, does not vary in time. In particular, Codd and Callaghan [3] develop analytic forms for the matrices A, S and R in geometries such as planar, cylindrical, and spherical pores, and analyse the effect of restricted diffusion when the gradient is perpendicular to the restricting boundary. Codd et al. do state that their method extends to varying gradient orientation, but they do not demonstrate the extension, which is non-trivial.

Pulse sequences with time-varying gradient orientation are becoming more common. For example the double pulsed field gradient (dPFG) pulse sequence [6], has received considerable interest recently because it may be sensitive to pore dimensions even at long diffusion wavelengths [4,6–10]. Furthermore, in MRI, imaging gradients and slice-select gradients can contribute significant diffusion weighting, but in general have orientation which is often different from that of the diffusion gradients.

Very few methods exist that can simulate signal from diffusion sequences with varying gradient orientation. Özarslan and Basser [7] propose an analytic approximation to the matrix formalism that does allow varying orientation. However, the approximation is valid only in the "low q-regime" [7], i.e. for small amounts of diffusion weighting. To avoid this serious limitation, later work [11] proposes an alternative general framework based on the multiple correlation function (MCF) approach of Grebenkov [12]. Monte Carlo simulations [13,14] can also be used for simulating diffusion signal under gradients with time-varying orientation. Monte Carlo simulations have the advantage that they can simulate diffusion in very complex systems, see for example [15], however they are computationally very expensive and, in particular, are impractical for model fitting and parameter estimation.

* Corresponding author. Address: University College London, Computer Science, Gower Street London, United Kingdom.
E-mail address: i.drobnjak@cs.ucl.ac.uk (I. Drobnjak).

1090-7807/$ - see front matter © 2011 Elsevier Inc. All rights reserved.
doi:10.1016/j.jmr.2011.02.022

Here we demonstrate an efficient implementation of the matrix formalism for the time-varying case and arbitrary diffusion weighting. The extension requires 3D rather than 1D solutions of the diffusion equation. More importantly, however, a naive extension requires evaluation of the fundamental matrix A every time the orientation changes. We show how to avoid the recalculation and thus retain computational efficiency similar to the fixed-orientation case. A key motivation is to extend earlier optimisation work [5] to gradient waveforms that can vary in orientation during the pulse sequence. The new implementation also enables efficient model fitting to data acquired using the output of this kind of optimisation. We demonstrate the correctness of the extended matrix formalism method by comparison with Monte Carlo simulations, focusing on the cylindrical geometry; we provide the corresponding expressions for the planar and spherical geometries in Appendix A.

2. Theory

2.1. Brief review of the matrix formalism for fixed gradient orientation

The matrix formalism in its general form has been described in detail elsewhere [1] and will be outlined only briefly here. In order to calculate the diffusion signal under generalised gradients, the gradient waveform $\mathbf{g}$ is approximated by a finely sampled succession of impulses. This subdivides the diffusion process into a sequence of time intervals, with fixed length τ, bounded by the gradient impulses $\mathbf{q}$. Spin phase evolutions take place at the boundaries of the intervals, and diffusion occurs during the intervening periods. The gradient amplitude $\mathbf{g}(n\tau)$, $n \in \{1, 2, \ldots, N+1\}$ is quantised into steps of size $\mathbf{g}_{step}$. This way, at time $n\tau$ the impulse is

$$\mathbf{q}_n = m_n \mathbf{q} \tag{2}$$

where

$$\mathbf{q} = (2\pi)^{-1}\gamma\tau\mathbf{g}_{step} \tag{3}$$

$$m_n = integ(\mathbf{g}(n\tau)/\mathbf{g}_{step}), \tag{4}$$

and $\gamma = 2.675 \times 10^8$ rad T^{-1} s^{-1} is the nuclear gyromagnetic ratio. The signal at the echo time is then

$$\begin{aligned} E = \int\int\cdots\int \rho(\mathbf{r}_1)\exp(i2\pi\mathbf{q}_1\cdot\mathbf{r}_1)P(\mathbf{r}_1|\mathbf{r}_2,\tau) \\ \times \exp(i2\pi\mathbf{q}_2\cdot\mathbf{r}_2)P(\mathbf{r}_2|\mathbf{r}_3,\tau)\cdots\times\exp(i2\pi\mathbf{q}_N\cdot\mathbf{r}_N)P(\mathbf{r}_N|\mathbf{r}_{N+1},\tau) \\ \times \exp(i2\pi\mathbf{q}_{N+1}\cdot\mathbf{r}_{N+1})\,d\mathbf{r}_1\,d\mathbf{r}_2\ldots d\mathbf{r}_{N+1} \end{aligned} \tag{5}$$

where $P(\mathbf{r}|\mathbf{r}', \tau)$ is the diffusion propagator which gives the probability that a spin starting at position $\mathbf{r}$ will move to $\mathbf{r}'$ after a time interval τ. The differential equation governing $P(\mathbf{r}|\mathbf{r}', \tau)$ is Fick's law, $D_r\Delta P = \partial P/\partial t$, where D_r is the diffusion constant [1]. For restricted diffusion, the eigenmode expansion describes the diffusion propagator conveniently:

$$P(\mathbf{r}|\mathbf{r}', t) = \sum_{n=0}^{\infty}\exp(-\lambda_n t)u_n(\mathbf{r})u_n^*(\mathbf{r}') \tag{6}$$

where u_n are an orthonormal set of solutions to the Helmholtz equation (obtained from Fick's equation by standard methods of separation of $\mathbf{r}$ and t variables [16]) parametrized with corresponding eigenvalues λ_n;u_n and λ_n depend only on the restricting geometry. The signal E can then be written as a matrix product

$$E = S(\mathbf{q}_1)RA(\mathbf{q}_2)RA(\mathbf{q}_3)\ldots RA(\mathbf{q}_N)RS^*(-\mathbf{q}_{N+1}) \tag{7}$$

where the elements of the matrices S, A and R are

$$S_v(\mathbf{q}) = V^{-1/2}\int u_v(\mathbf{r})\exp(i2\pi\mathbf{q}\cdot\mathbf{r})\,d\mathbf{r} \tag{8}$$

$$R_{vv} = \exp(-\lambda_v\tau) \tag{9}$$

$$A_{v\mu}(\mathbf{q}) = \int u_v^*(\mathbf{r})u_\mu(\mathbf{r})\exp(i2\pi\mathbf{q}\cdot\mathbf{r})\,d\mathbf{r} \tag{10}$$

v, $\mu \in \{1, 2, \ldots\}$ and V is the pore volume. Note that S is a column vector and R is a diagonal matrix. Using Eq. (2) together with the formula $A(n\mathbf{q}) = A(\mathbf{q})^n$ (proved in [1]) the total signal simplifies to

$$E = S(\mathbf{q})RA(\mathbf{q})^{m_2}RA(\mathbf{q})^{m_3}\ldots RA(\mathbf{q})^{m_N}RS^*(\mathbf{q}) \tag{11}$$

where m_n, $n \in \{2, \ldots, N\}$ are defined in Eq. (4). This way any gradient waveform can be handled provided that we calculate just three matrices $A(\mathbf{q})$, $S(\mathbf{q})$ and $R(\tau)$, where $\mathbf{q}$ is the smallest impulse used to digitise the waveform. Codd and Callaghan [3] derive expressions for the matrices $A(\mathbf{q})$, $S(\mathbf{q})$ and $R(\tau)$ for planar, cylindrical and spherical geometry and use the above theory straightforwardly.

2.2. Extension for the gradients with time-varying orientation

In the review of the matrix formalism in the previous section, the gradient orientation is implicitly fixed throughout the pulse sequence. The vector $\mathbf{q}$, defined by Eq. (3), is the same at every time point $n\tau$, $n \in \{1, 2, \ldots, N+1\}$, and it is precisely this that allows a single calculation of matrices $A(\mathbf{q})$ and $S(\mathbf{q})$ when evaluating Eq. (11). However, if the gradient orientation varies in time, the orientation of $\mathbf{q}$ must vary as well and Eqs. (2) and (3) need to be redefined as:

$$\mathbf{q}_n = |\mathbf{q}_n|\hat{q}_n, \quad |\mathbf{q}_n| = m_n|\mathbf{q}| \tag{12}$$

where

$$|\mathbf{q}| = (2\pi)^{-1}\gamma\tau|\mathbf{g}_{step}|, \quad m_n = integ(|\mathbf{g}(n\tau)|/|\mathbf{g}_{step}|) \tag{13}$$

and $\hat{q}_n$ is the unit vector, defined for every time point $n\tau$, $n \in \{1, 2, \ldots, N+1\}$, along the direction of $\mathbf{q}_n$. Now, the total signal is

$$E = S(|\mathbf{q}|\hat{q}_1)RA(|\mathbf{q}|\hat{q}_2)^{m_2}R\ldots RA(|\mathbf{q}|\hat{q}_N)^{m_N}RS^*(|\mathbf{q}|\hat{q}_{N+1}) \tag{14}$$

which is equivalent to Eq. (11), but for the case when the gradient orientation varies throughout the pulse sequence.

Eq. (11) requires matrices $A(\mathbf{q})$ and $S(\mathbf{q})$ to be calculated only once for a given geometry while Eq. (14) requires a separate calculation of each $A(|\mathbf{q}|\hat{q}_n)$, $n \in \{2, 3, \ldots, N\}$ and $S(|\mathbf{q}|\hat{q}_n)$, $n \in \{1, N+1\}$. Element by element, calculation of each matrix is computationally too expensive for the whole process to be practical. The 3D extension we present below calculates these matrices efficiently.

2.3. Demonstration for the case of cylindrical geometry

First we introduce cylindrical polar coordinates in which the longitudinal z-axis is a symmetry axis for the system and the relevant polar coordinates are (r, θ) where $r \in [0, a]$, $\theta \in [0, 2\pi]$ and a is the radius of the cylinder. The eigenvectors become:

$$u_v(r, \theta) = \alpha_{nn'}J_n\left(\beta_{nn'}\frac{r}{a}\right)\exp(in\theta) \tag{15}$$

where $\alpha_{nn'}$ are the normalisation constants

$$\alpha_{nn'} = \sqrt{\frac{\beta_{nn'}^2}{\pi a^2 J_n^2(\beta_{nn'})(\beta_{nn'}^2 - n^2)}} \tag{16}$$

J_n are standard (cylindrical) Bessel functions of order n, $\beta_{nn'}$ is the n'th root of the equation $J_n'(\beta_{nn'}) = 0$ [1,3], and $v \in \{1, 2, 3\ldots\}$ is an index representing the position of a given root in a sorted, ascending, sequence of roots $\{\beta_{nn'}|\ \forall n, n'\}$. Note that the eigenvectors here are different from the ones in Codd and Callaghan [3]. The last term

in Eq. (15) is a complex exponential which allows any gradient orientation, while [3] states just its real part which only allows for the gradient orientation to be aligned with the x-axis. As a result, the normalisation constants, which were calculated using the L^2 norm of the eigenvectors, are also different. Here, they have exactly the same form for all n but in [1,3] the cases for $n = 0$ and $n \neq 0$ differ. The normalisation constants here are the same as those from [1,3] for $n = 0$. The eigenvalues are the same as in [1,3]

$$\lambda_v = \frac{\beta_{nn'}^2 D_r}{a^2} \tag{17}$$

We consider only the x–y component of the gradient impulses $\mathbf{q}_n$ because no restriction occurs along the cylinder's axis (z-axis). According to Eqs. (12) and (13), at each time interval τ we can quantise $\mathbf{q}_n$ using $\mathbf{q} = (q,\theta_q)$ where q is the amplitude and the θ_q is the angle between the gradient and the x-axis. Now the matrices can be written as

$$S_v(q,\theta_q) = V^{-\frac{1}{2}}\alpha_{nn'}\int_0^a J_n\left(\beta_{nn'}\frac{r}{a}\right)r\int_0^{2\pi}\exp(in\theta) \times \exp(i2\pi qr\cos(\theta-\theta_q))\,\mathrm{d}\theta\,\mathrm{d}r$$

$$R_{vv} = \exp\left(-\frac{\beta_{nn'}^2 D_r}{a^2}\tau\right)$$

$$A_{v\mu}(q,\theta_q) = \alpha_{nn'}\alpha_{kk'}\int_0^a J_n\left(\beta_{nn'}\frac{r}{a}\right)J_k\left(\beta_{kk'}\frac{r}{a}\right)r\int_0^{2\pi} \times \exp(i(k-n)\theta)\exp(i2\pi qr\cos(\theta-\theta_q))\,\mathrm{d}\theta\,\mathrm{d}r \tag{18}$$

We can choose q so that $qr \ll 1$ (we find $qr = O(10^{-3})$ sufficient) and thus use the 1st order Taylor expansion

$$\exp(i2\pi qr\cos(\theta-\theta_q)) \approx 1 + i2\pi qr\cos(\theta-\theta_q) \tag{19}$$

to obtain

$$A_{v\mu}(q,\theta_q) = \begin{cases} 2\pi\alpha_{nn'}\alpha_{kk'}\int_0^a J_n(\beta_{nn'}\frac{r}{a})J_k(\beta_{kk'}\frac{r}{a})r\,\mathrm{d}r & n=k \\ 2\pi^2\alpha_{nn'}\alpha_{kk'}q(\mp\sin\theta_q + i\cos\theta_q)\int_0^a J_n(\beta_{nn'}\frac{r}{a})J_k(\beta_{kk'}\frac{r}{a})r^2\,\mathrm{d}r & n=k\pm1 \\ 0 & n\neq k,k\pm1 \end{cases}$$

$$S_v(q,\theta_q) = \begin{cases} V^{-\frac{1}{2}}2\pi\alpha_{nn'}\int_0^a J_n(\beta_{nn'}\frac{r}{a})r\,\mathrm{d}r & n=0 \\ V^{-\frac{1}{2}}2\pi^2\alpha_{nn'}q(\sin\theta_q + i\cos\theta_q)\int_0^a J_n(\beta_{nn'}\frac{r}{a})r^2\,\mathrm{d}r & n=1 \\ 0 & n>1 \end{cases} \tag{20}$$

Thus we see that

$$A_{v\mu}(q,\theta_q) = \mathrm{Re}[A_{v\mu}(q,0)] + \mathrm{sign}(k-n)\ \mathrm{Im}[A_{v\mu}(q,0)]\sin\theta_q + i\mathrm{Im}[A_{v\mu}(q,0)]\cos\theta_q$$

$$S_v(q,\theta_q) = \mathrm{Re}[S_v(q,0)] + \mathrm{Im}[S_v(q,0)]\sin\theta_q + i\ \mathrm{Im}[S_v(q,0)]\cos\theta_q \tag{21}$$

Eq. (21) are the key equations in the implementation of the method for varying orientation. They show that each A and S is simply a linear combination of the real and the imaginary parts of fundamental matrices $A(q,0)$ and $S(q,0)$. We calculate the fundamental matrices, which require expensive numerical integrals, only once and calculate the total signal as in Eq. (14). We define similar expressions for planar and spherical geometry in Appendix A.

3. Experiments and results

This section shows three experiments to validate the new implementation against Monte Carlo simulations. The first experiment use the dPFG sequence, the second helical waveforms and the third a stimulated echo diffusion sequence (STEAM).

We determine the dimension of the matrices by the convergence criteria when multiplying out the products, which is the speed by which the exponents of the elements of the R matrix decay [1]. For $k \times k$ matrices the R matrix elements will decay as $\exp(-k^2\pi^2 D_r\tau/a^2)$. Similar to Codd and Callaghan [3] we have found 20×20 matrices sufficiently accurate for our purposes.

Monte Carlo simulations use the Camino diffusion simulations system [13]. We run simulations of molecules trapped within cylinders (no other compartments) and each simulation uses 160,000 walkers and 5000 time steps.

3.1. dPFG sequence

The dPFG sequence [6] is characterised by two distinct PGSE blocks, which are separated from each other by the mixing time t_m, as shown in Fig. 1a top. Each PGSE block has diffusion time Δ and each diffusion gradient is assumed to have the same pulse duration δ. The angle ψ is the angle between the vectors $\mathbf{G}_1$ and $\mathbf{G}_2$ (Fig. 1a bottom). The amplitudes $G_1 = |\mathbf{G}_1|$ and $G_2 = |\mathbf{G}_2|$ of the two vectors are the same for all the experiments. To compare our results to existing experimental results, we choose the same experimental design as in [10,11], which plot signals from spectroscopy on water filled microcapillaries. In all the experiments, only the signal from the intra-cylinder space is calculated.

Fig. 1b shows the results for $\delta = \{1.5, 4.5, 7.5\}$ ms and for a range of angles $\psi \in [0, 360]$ degrees. The rest of the pulse sequence parameters used were $G_1 = G_2 \in \{0.3757,\ 0.1252, 0.0751\}$ T/m (one for each δ value respectively), $\Delta = 40$ ms, $t_m = 0$. The model parameters were: the diffusion constant $D_r = 2 \times 10^{-9}$ m^2/s and the cylinder radius $R = 5.2$ μm.

Fig. 1c shows the results for $G_1 = G_2 \in \{0.1377, 0.2567, 0.3757\}$ T/m and for a range of angles $\psi \in [0, 360]$ degrees. The rest of the pulse sequence parameters were $\delta = 1.5$ ms, $\Delta = 120$ ms, $t_m = 0$. This time $D_r = 2 \times 10^{-9}$ m^2/s and $R = 9.7$ μm.

Fig. 1d shows the results for $t_m = \{0, 5, 20, 100\}$ ms and for a range of angles $\psi \in [0, 360]$ degrees. The rest of the pulse sequence parameters used were $\delta = 1.5$ ms, $\Delta = 40$ ms, $G_1 = G_2 = 0.3757$ T/m. This time $D_r = 2 \times 10^{-9}$ m^2/s and $R = 5.2$ μm.

All the experiments show excellent agreement between matrix formalism method and the Monte Carlo simulations, see Fig. 1. Normalised Root Mean Square Error (NRMS) for each of the plots is below 1%. The results also show excellent agreement with the published experimental results [10,11].

3.2. Helical waveforms

We invented the helix sequence just for the purposes of the validation. This sequence generalises oscillating gradient spin echo (OGSE) sequence by allowing the gradient orientation to vary in time. It is a useful test as the gradient orientation changes continually through the waveform unlike the other two sequences, which have piecewise constant waveforms. We define the waveform as

$$\mathbf{G}(t) = \left[\cos\frac{2\pi(t-\tau_1)f}{T},\ \sin\frac{2\pi(t-\tau_1)f}{T},\ \frac{t-\tau_1}{5T}\right]G, \quad \tau_1 < t < \tau_1 + T \tag{22}$$

where τ_1 is the time between the 90 degree RF pulse and the gradient, T is the duration of the gradient, f is the frequency of oscillations and G modifies the amplitude of the gradient. The second part of the waveform after the 180 degree pulse, is identical to the first and starts at time τ_2 after the first part. The diagram of the waveform can be found in Fig. 2a.

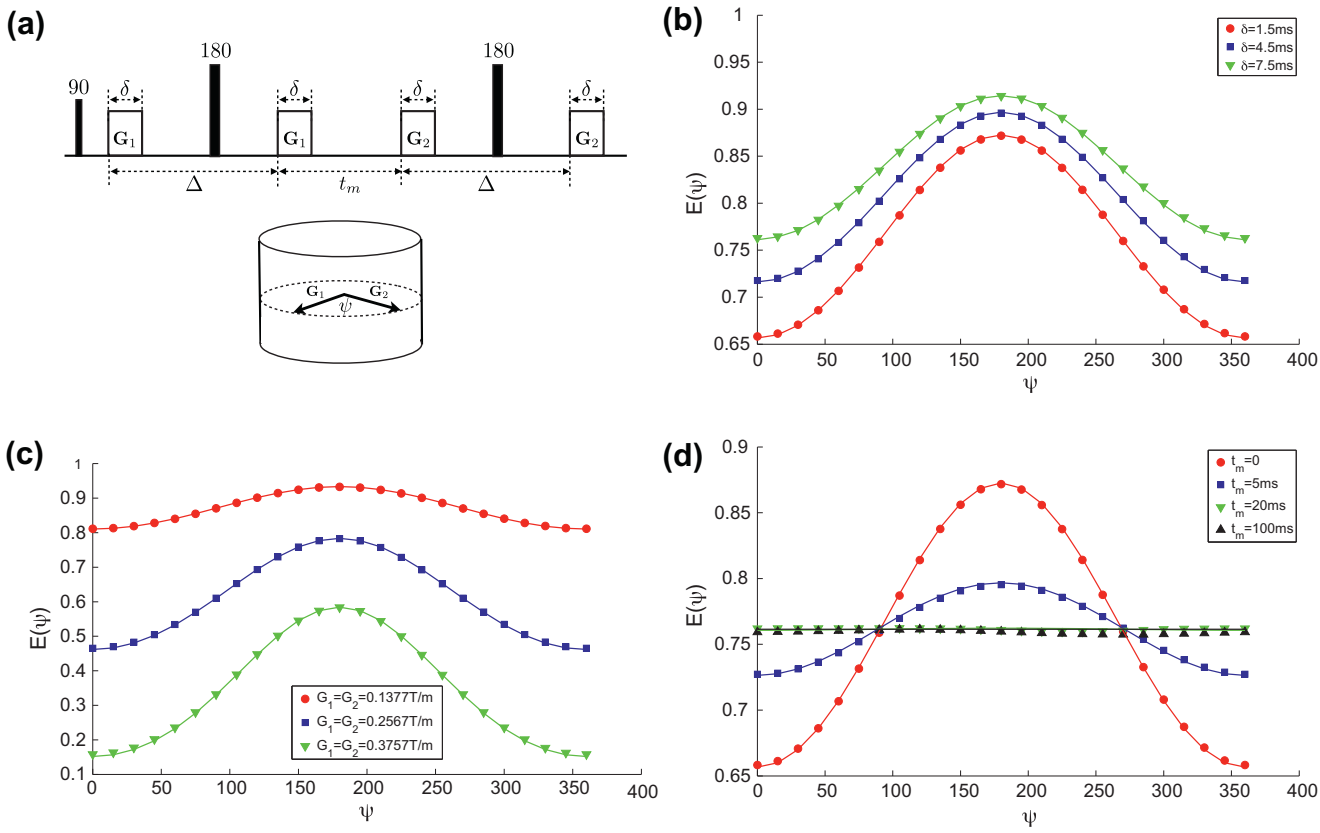

Fig. 1. Validation results for the double-PFG sequence. Full lines are the matrix formalism simulations, points on the lines are the Monte Carlo simulations. The diagram of the sequence is shown in (a) top, while (a) bottom shows the angular relationship between the vectors $\mathbf{G}_1$ and $\mathbf{G}_2$. For all of the experiments $\mathbf{G}_1$ is set along the x-axis while $\mathbf{G}_2$ is varied in the x–y plane with $\psi \in [0,360]$degrees. In each plot a different parameter was varied: (b) the duration of the gradient pulses δ; (c) the strength of the gradients G_1 and G_2; (d) the mixing time t_m. The values of the rest of the parameters are specified in the main text.

Fig. 2b shows the results for $G \in \{0.05, 0.08, 0.15\}$ T/m and for a range of frequencies $f \in [0.2, 3]$. The rest of the parameters used were $\tau_1 = 1$ ms, $\tau_2 = 2.7$ ms $T = 10$ ms, $D_r = 2 \times 10^{-9}$ m^2/s and $R = 5$ μm.

The agreement between the matrix formalism (full lines) and the Monte Carlo simulations (marked points) is excellent. The NRMS for each of the three plots is below 0.9%.

3.3. STEAM sequence

The stimulated echo (STEAM) sequence [17] has two 90 degree RF pulses, instead of the single 180 degree pulse in the more common PGSE sequence, to allow longer diffusion times without T_2 decay. However, crusher $\mathbf{G}_c$ and slice-select gradients $\mathbf{G}_s$ around the second and third 90 degree pulses add significant diffusion weighting in the slice direction, much more so than in PGSE because they are separated by the mixing time. Fig. 3a shows a diagram of the sequence. The main goal of this section is to validate the method for sequences which have the imaging gradients (crusher and slice-select gradients), which are differently oriented from the diffusion gradients. However, we also run simulations for the same sequences, just without the imaging gradients, to show what difference that makes in the signal.

Fig. 3b shows the simulated signal for fifty different measurements from a single-shell HARDI protocol implemented on a high field preclinical scanner. Orientation of the diffusion gradients is randomly distributed over a hemisphere and is different for each of the measurements but the magnitude is constant. In all measurements, $\delta_s = 1$ ms, $\delta_c = 1.5$ ms, $\delta_d = 7.9$ ms, $\tau_1 = \tau_2 = 0$ ms, $G_d = 0.14$ T/m and the crusher and the slice-select gradients $\mathbf{G}_c$, $\mathbf{G}_s$ are oriented along the z-axis with intensities $G_c = 0.04$ T/m, $G_s = 0.139$ T/m.

Fig. 3b shows that the matrix formalism simulations (full lines) agree very clearly with the Monte Carlo simulations (marked points). The NRMS is below 0.51%. The dashed line shows the matrix formalism simulations if imaging gradients are ignored, i.e. $G_s = G_c = 0$. The points with the opposite bias, i.e. the ones above the dashed curve, are measurements acquired with sequences in which $\mathbf{G}_{dz}$ (the projection of $\mathbf{G}_d$ in z direction) and $\mathbf{G}_c$ are of opposite sign. Due to the cancelation of these gradients, the diffusion weighting is smaller than in measurements with no imaging gradients.

The difference between the full and the dashed lines is clear and the NRMS for this experiment is at 7%. These results suggest that imaging gradients should be accounted for when using the STEAM sequence.

4. Discussion

Here we generalise the numerical matrix formalism of Codd and Callaghan [3] to gradient waveforms with time-varying orientation. The two key differences are: (1) derivation of eigenvectors for varying orientation; (2) the evaluation of the matrices A and S to express $A(q, \theta_q)$ and $S(q, \theta_q)$ as simple functions of $A(q, 0)$ and $S(q, 0)$. This makes the simulation of the time-varying gradient orientation sequences computationally practical. We approximate each sequence with hundreds of impulses and the evaluation of each signal takes just a few minutes. The computational demands, because of the nature of the method, are almost the same as for the 1D case. The only extra calculation is the implementation of Eq. (21) at each time step to accommodate the change in the gradient

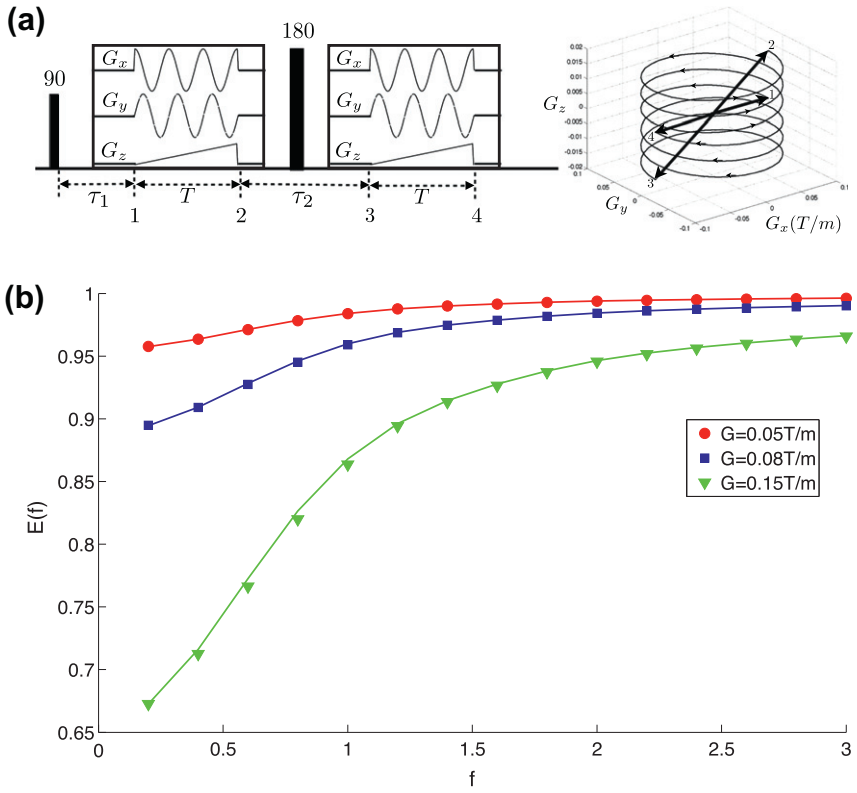

Fig. 2. Validation results for the helical waveforms. The gradient vectors are rotating in a shape of a helix with frequency $f \in [0.2, 3]$ as described with Eq. (22). A diagram of the sequence is shown in (a), where positions 1, 2, 3 and 4 mark the gradient vector $\mathbf{G} = [G_x, G_y, G_z]$ at the beginning of the sequence, just before the 180 degree RF pulse, just after, and at the end of the sequence respectively. Full lines in (b) are the matrix formalism simulations, points on the lines are the Monte Carlo simulations. Each line is generated with a different gradient amplitude determined by G as shown in Eq. (22). The rest of the parameters are outlined in the main text.

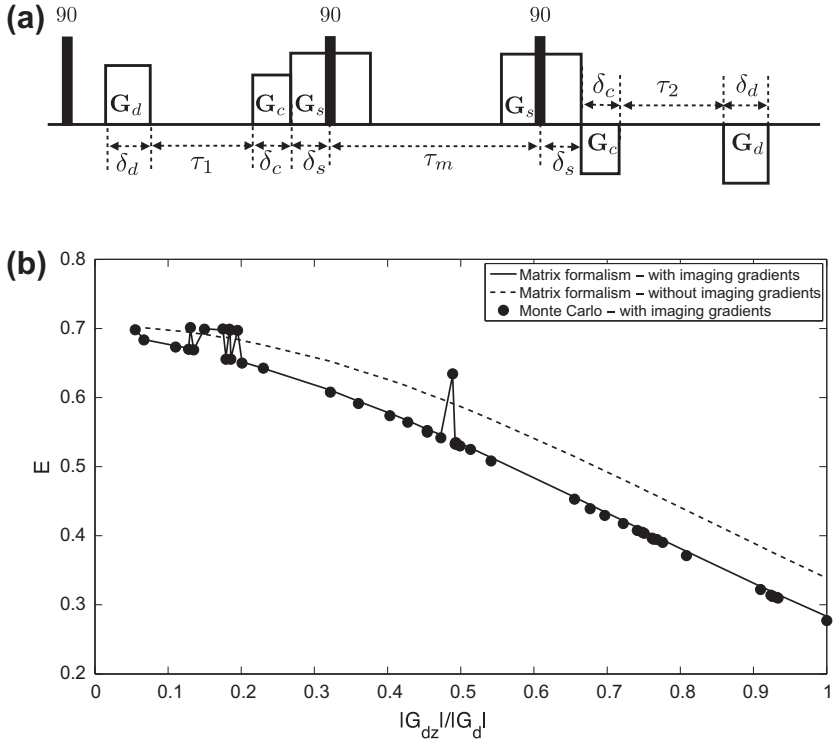

Fig. 3. Validation results for the STEAM sequence (shown in (a)). In (b) full lines are the matrix formalism simulations with imaging gradients (slice-select $\mathbf{G}_s$ and the crusher gradient $\mathbf{G}_c$), dashed lines are without, i.e. $G_s = G_c = 0$, and the marker points are the Monte Carlo simulations with imaging gradients. $\mathbf{G}_s$, $\mathbf{G}_c$ are oriented along the z-axis and $\mathbf{G}_{dz}$ is the projection of the diffusion gradient $\mathbf{G}_d$ in z direction. The parameter values are specified in the main text.

direction if present. We demonstrated the approach for cylindrical geometry and validate it in simulation using three different protocols: dPFG, STEAM and helical waveforms. Predicted signal is highly consistent with simulation.

Unlike the analytic approximation in [18], our approach extends the matrix formalism to gradient waveforms with time-varying orientation that support arbitrary diffusion weighting. In [18] each $|\mathbf{q}_n| = m_n|\mathbf{q}|$, i.e. the diffusion weighting of the whole waveform, needs to be small. Our method only requires that the impulse increments $|\mathbf{q}|r$ are small. This assumption is easily satisfied by choosing τ and $|\mathbf{g}_{step}| \ll 1$ as $|\mathbf{q}| = (2\pi)^{-1}\gamma\tau|\mathbf{g}_{step}|$.

Our approach is also different from the generalised MCF method [11], which allows time-varying gradient orientation and has no restrictions on the diffusion weighting. The main difference is in how the NMR signal from a general gradient waveform is computed. The matrix formalism approximates the gradient waveform as a sequence of impulses and utilize the propagator method, yielding the signal as the product of a set of matrices. In contrast, the MCF method approximates the gradient waveform using a piecewise-constant function and explicitly solves the Bloch–Torrey equation, yielding the signal as the product of a set of matrix exponentials. MCF method offers itself very naturally for application where the gradient behaviour can be described in blocks, hence application to the dPFG sequence or for modelling imaging gradients appears ideal. Our work extending [5] however, focusses on optimising a very general form of the gradient waveform. The matrix formalism offers itself more naturally to our application as it allows continuous changes in the amplitude and orientation, with no computational penalty. With our extension, computational complexity of the MCF and matrix method appear similar, although future work is required to perform a formal comparison.

Here, we considered only very simple geometries such as cylinders and spheres but the method adapts for other geometries. Also, the first order approximation in Eq. (19) is a potential source of inaccuracy. However, when we include the second order term in the calculations we see little improvement to the already accurate results. Finally, we have not considered surface relaxation here. Our extension adapts easily by modifying appropriately the roots and the normalisation constants of the basic matrices. It does not interfere with the calculations when the gradient direction is changing.

Acknowledgments

We thank Noam Shemesh for providing us with the experimental parameters for the dPFG sequence. We also thank EPSRC (EP/E007748) and CONNECT (EU FP7 framework) for providing the funding for this project.

Appendix A

A.1. Planar geometry

In the case of planar geometry Codd and Callaghan [3] gives analytical expressions for matrices A, S and R when the gradient is applied along the z-axis normal to a pair of parallel planes. When the gradient changes orientation during the sequence, it is possible to decompose the gradient vector into components parallel and perpendicular to the plates, so the signal can be written as the product of the contributions from restricted and free diffusions. The contribution to the signal attenuation from restricted diffusion can be obtained from Eq. (11), and the effect of the orientation change in the gradient will be present only in the indexes m_n as these will be modified with the modification of the $\mathbf{q}_n$ amplitude along the z-axis. Because of this, there is no need to discuss the planar geometry further here, and the formulas from [3] can be used straightforwardly.

A.2. Spheres

We introduce spherical polar coordinates $x = r\cos\theta$, $y = r\sin\theta\cos\phi$, $z = r\sin\theta\sin\phi$ where $r \in [0, a]$, $\theta \in [0, \pi]$, $\phi \in [0, 2\pi]$ and a is the radius of the sphere. In a similar fashion as in the cylindrical case, just in spherical polar coordinates, we solve the Helmholtz equation to get an orthonormal set of eigenvectors:

$$u_v(r,\theta) = \alpha_{njm} j_n\left(\beta_{nj}\frac{r}{a}\right) P_n^{|m|}(\cos\theta)\exp(im\phi) \tag{23}$$

where $n = 0, \ldots, \infty$, $j = 0, \ldots, \infty$, $m = -n, \ldots, 0, \ldots, n$ and α_{njm} are the normalisation constants

$$\alpha_{njm} = \sqrt{\frac{(2n+1)(n-m)!}{4\pi^2 a^3 (n+m)!(j_n^2(\beta_{nj}) - j_{n-1}(\beta_{nj})j_{n+1}(\beta_{nj}))}}, \tag{24}$$

j_n are spherical Bessel functions of order n, β_{nj} is the jth root of the equation $j_n'(\beta_{nj}) = 0$ and $v \in \{1, 2, 3 \ldots\}$ is an index representing the position of a given root in a sorted, ascending, sequence of roots $\{\beta_{nn'} | \forall n, n'\}$. Note that the last term in the eigenvector depends on the azimuthal angle ϕ and this term does not exist in [3]. Since the gradients were assumed to be applied along the x direction in [3], the result was independent of the azimuthal angle and the associated state index m. However, this is no longer the case if we allow the gradients to be applied along other directions. The eigenvalues are

$$\lambda_v = \frac{\beta_{nj}^2 D_r}{a^2} \tag{25}$$

The quantised impulse at each time interval τ is $\mathbf{q}$, which in spherical coordinate system equals $(q\cos\theta_q, q\sin\theta_q\cos\phi_q, q\sin\theta_q\sin\phi_q)$ and hence

$$\mathbf{q}\cdot\mathbf{r} = qr(\cos\theta\cos\theta_q + \sin\theta\sin\theta_q\cos\phi\cos\phi_q + \sin\theta\sin\theta_q \times \sin\phi\sin\phi_q) \tag{26}$$

With some trigonometric manipulation, the matrices can now be written as

$$S_v(q,\theta_q,\phi_q) = V^{-\frac{1}{2}}\alpha_{njm}\int_0^a j_n(\beta_{nj}\frac{r}{a})r^2\int_0^\pi P_n^{|m|}(\cos\theta)\sin\theta \times \int_0^{2\pi}\exp(im\phi)\exp(i2\pi qr(\cos\theta\cos\theta_q + \sin\theta\sin\theta_q\cos(\phi-\phi_q)))\,\mathrm{d}\phi\,\mathrm{d}\theta\,\mathrm{d}r$$

$$R_{vv} = \exp\left(-\frac{\beta_{nn'}^2 D_r}{a^2}\tau\right)$$

$$A_{v\mu}(q,\theta_q,\phi_q) = \alpha_{njm}\alpha_{n'j'm'}\int_0^a j_n(\beta_{nj}\frac{r}{a})j_{n'}(\beta_{n'j'}\frac{r}{a})r^2 \times \int_0^\pi P_n^{|m|}(\cos\theta)P_{n'}^{|m'|}(\cos\theta)\sin\theta \times \int_0^{2\pi}\exp(i(m'-m)\phi)\exp(i2\pi qr(\cos\theta\cos\theta_q + \sin\theta\sin\theta_q\cos(\phi-\phi_q)))\,\mathrm{d}\phi\,\mathrm{d}\theta\,\mathrm{d}r \tag{27}$$

In the same way as for the cylinders we use the 1st order Taylor expansion for the last exponential in the integrals and now the matrices A and S become:

$$A_{v\mu}(q,\theta_q,\phi_q)=\begin{cases}2\pi\alpha_{njm}\alpha_{n'j'm'}\int_0^a j_n(\beta_{nj}\frac{r}{a})j_{n'}(\beta_{n'j'}\frac{r}{a})r^2\,\mathrm{d}r\\ \times\int_0^\pi P_n^{|m|}(\cos\theta)P_{n'}^{|m'|}(\cos\theta)\sin\theta\,\mathrm{d}\theta\\ +i\cos\theta_q q4\pi^2\alpha_{njm}\alpha_{n'j'm'}\int_0^a j_n(\beta_{nj}\frac{r}{a})j_{n'}(\beta_{n'j'}\frac{r}{a})r^3\,\mathrm{d}r\\ \times\int_0^\pi P_n^{|m|}(\cos\theta)P_{n'}^{|m'|}(\cos\theta)\sin\theta\cos\theta\,\mathrm{d}\theta & m'-m=0\\ \sin\theta_q(\mp\sin\phi_q+i\cos\phi_q)q2\pi^2\alpha_{njm}\alpha_{n'j'm'}\\ \times\int_0^a j_n(\beta_{nj}\frac{r}{a})j_{n'}(\beta_{n'j'}\frac{r}{a})r^3\,\mathrm{d}r\\ \times\int_0^\pi P_n^{|m|}(\cos\theta)P_{n'}^{|m'|}(\cos\theta)\sin^2\theta\,\mathrm{d}\theta & m'-m=\pm1\\ 0 & m'-m\neq0,\ \pm1\end{cases}\tag{28}$$

$$S_v(q,\theta_q,\phi_q)=\begin{cases}V^{-\frac{1}{2}}2\pi\alpha_{njm}\int_0^a j_n(\beta_{nj}\frac{r}{a})r^2\,\mathrm{d}r\\ \times\int_0^\pi P_n^{|m|}(\cos\theta)\sin\theta\,\mathrm{d}\theta\\ +i\cos\theta_q q4\pi^2\alpha_{njm}\int_0^a j_n(\beta_{nj}\frac{r}{a})r^3\,\mathrm{d}r\\ \times\int_0^\pi P_n^{|m|}(\cos\theta)\sin\theta\cos\theta\,\mathrm{d}\theta & m=0\\ V^{-\frac{1}{2}}\sin\theta_q(\sin\phi_q+i\cos\phi_q)q2\pi^2\alpha_{njm}\\ \times\int_0^a j_n(\beta_{nj}\frac{r}{a})r^3\,\mathrm{d}r\\ \times\int_0^\pi P_n^{|m|}(\cos\theta)\sin^2\theta\,\mathrm{d}\theta & m=1\\ 0 & m\neq0,1\end{cases}\tag{29}$$

Thus we see that

$$\begin{aligned}A_{v\mu}(q,\theta_q,\phi_q)=\mathrm{Re}[A_{v\mu}(q,0,0)]+\ &\mathrm{sign}(m-m')\mathrm{Im}[A_{v\mu}(q,\pi/2,0)]\\ &\times\sin\phi_q+i(\mathrm{Im}[A_{v\mu}(q,0,0)]\cos\theta_q\\ &+\ \mathrm{Im}[A_{v\mu}(q,\pi/2,0)]\cos\phi_q)\end{aligned}$$

$$\begin{aligned}S_v(q,\theta_q,\phi_q)=\mathrm{Re}[S_v(q,0,0)]+\ &\mathrm{Im}[S_v(q,\pi/2,0)]\sin\phi_q\\ &+i(\mathrm{Im}[S_v(q,0,0)]\cos\theta_q+\ \mathrm{Im}[S_v(q,\pi/2,0)]\\ &\times\cos\phi_q)\end{aligned}\tag{30}$$

Matrices $A(q,0,0)$, $A(q,\pi/2,0)$ and $S(q,0,0)$, $S(q,\pi/2,0)$ are calculated only once at the beginning, while all the others are simply derived from them at steps where the orientation is changing. The signal is then calculated as in Eq. (14).

References

[1] P.T. Callaghan, A simple matrix formalism for spin echo analysis of restricted diffusion under generalized gradient waveforms, J. Magn. Reson. 129 (1) (1997) 74–84.
[2] A. Caprihan, L. Wang, E. Fukushima, A multiple-narrow-pulse approximation for restricted diffusion in a time-varying field gradient, J. Magn. Reson., Ser. A 118 (1) (1996) 94–102.
[3] S.L. Codd, P.T. Callaghan, Spin echo analysis of restricted diffusion under generalized gradient waveforms: planar, cylindrical, and spherical pores with wall relaxivity, J. Magn. Reson. 137 (2) (1999) 358–372.
[4] E. Özarslan, P.J. Basser, MR diffusion–'diffraction" phenomenon in multi-pulse-field-gradient experiments, J. Magn. Reson. 188 (2) (2007) 285–294.
[5] I. Drobnjak, B. Siow, D.C. Alexander, Optimizing gradient waveforms for microstructure sensitivity in diffusion-weighted MR, J. Magn. Reson. 206 (2010) 41–51.
[6] P.P. Mitra, Multiple wave-vector extensions of the NMR pulsed-field-gradient spin-echo diffusion measurement, Phys. Rev. B 51 (21) (1995) 15074–15078.
[7] E. Özarslan, P.J. Basser, Microscopic anisotropy revealed by NMR double pulsed field gradient experiments with arbitrary timing parameters, J. Chem. Phys. 128 (2008) 154511.
[8] M.A. Koch, J. Finsterbusch, Compartment size estimation with double wave vector diffusion-weighted imaging, Magn. Reson. Med. 60 (1) (2008) 90–101.
[9] M.E. Komlosh, M.J. Lizak, F. Horkay, R.Z. Freidlin, P.J. Basser, Observation of microscopic diffusion anisotropy in the spinal cord using double-pulsed gradient spin echo MRI, Magn. Reson. Med. 59 (4) (2008) 803–809.
[10] N. Shemesh, E. Özarslan, P.J. Basser, Y. Cohen, Measuring small compartmental dimensions with low-q angular double-PGSE NMR: The effect of experimental parameters on signal decay, J. Magn. Reson. 198 (1) (2009) 15–23.
[11] E. Özarslan, N. Shemesh, P. Basser, A general framework to quantify the effect of restricted diffusion on the NMR signal with applications to double pulsed field gradient NMR experiments, J. Chem. Phys. 130 (2009) 104702.
[12] D. Grebenkov, NMR survey of reflected Brownian motion, Rev. Mod. Phys. 79 (2007) 1077–1137.
[13] M.G. Hall, D.C. Alexander, Convergence and parameter choice for Monte-Carlo simulations of diffusion MRI, IEEE Trans. Med. Imaging 28 (2009) 1354–1364.
[14] J.C. Ford, D.B. Hackney, Numerical model for calculation of apparent diffusion coefficients (ADC) in permeable cylinders – comparison with measured ADC in rat spinal cord white matter, Magn. Reson. Med. 37 (1997) 387–394.
[15] E. Panagiotaki, M.G. Hall, H. Zhang, B. Siow, M.F. Lythgoe, D.C. Alexander, High-fidelity meshes from tissue samples for diffusion MRI simulations, in: Medical Image Computing and Computer-assisted Intervention – MICCAI 2010, Lecture Notes in Computer Science 6362/2010, 2010, pp. 404–411.
[16] S.J. Farlow, Partial Differential Equations for Scientists and Engineers, Dover Publications, Inc, New York, 1993.
[17] K.D. Merboldt, W. Hanicke, J. Frahm, Diffusion imaging using stimulated echoes, Magn. Reson. Med. 19 (2) (1991) 233–239.
[18] E. Özarslan, Compartment shape anisotropy (CSA) revealed by double pulsed field gradient MR, J. Magn. Reson. 199 (2009) 56–67.